THE GEOLOGICAL SOCIETY OF AMERICA®

Progressive fracturing in alluvial clasts

Uri Shaanan[1,†], Amit Mushkin[1], Monica Rasmussen[2], Amir Sagy[1], Philip Meredith[3], Yoshitaka Nara[4], Russell Keanini[5], and Martha-Cary Eppes[2]

[1]*Geological Survey of Israel, 32 Yesha'ayahu Leibowitz, Jerusalem 9692100, Israel*
[2]*Department of Geography and Earth Sciences, University of North Carolina at Charlotte, Charlotte, North Carolina 28223, USA*
[3]*Rock and Ice Physics Laboratory, Department of Earth Sciences, University College London, Gower Street, London WC1E 6BT, UK*
[4]*Graduate School of Engineering, Kyoto University, Kyoto-Daigaku-Katsura, Nishikyo-ku, Kyoto 615-8540, Japan*
[5]*Department of Mechanical Engineering and Engineering Science, University of North Carolina at Charlotte, Charlotte, North Carolina 28223, USA*

ABSTRACT

Rock fracturing sets the pace for a range of geomorphic processes. While experimental studies and modeling have provided invaluable insights into the mechanisms and rates of rock fracturing as a function of stress, time, and environmental conditions, field-based observations of subaerial fracturing evolution over geologic time are scarce. To address this knowledge gap, we conducted a systematic study of fractures that developed subaerially and in situ within clasts perched on abandoned late Quaternary alluvial surfaces (ca. 0, ca. 14, and ca. 62 ka in age) in the hyperarid Dead Sea Rift Valley, Israel. Using quantitative field observations, petrographic, and scanning electron microscopy, and micron-scale laser scans of fracture surfaces we found that fractures exhibit a consistent pattern of three distinctive weathering zones: (1) an "Outer Zone," where fracture surface morphology resembles the clast exterior; (2) an "Accumulation Zone," where fractures are infilled by "loose" accumulated particles; and (3) an "Inner Zone" where fractures extend inward to the crack-tip and preferentially follow grain boundaries. Crack-tips are characterized as a distinct micro domain that consists of fracture-parallel microcracks, chemical alteration, and dissolution morphologies. Altogether, the laboratory results indicate chemically enhanced fracturing and infiltration of water ahead of traction-free, open crack-tips. Field measurements also revealed an increase in fracture number density over geologic time. Our results highlight new details regarding the progressive nature of mechanical weathering through geologic time and the role of moisture as a potential rate-setting factor in the fracturing that allows mechanical weathering.

INTRODUCTION

Mechanical weathering and specifically physical breakdown of rocks that are subaerially exposed is a fundamental process that often sets the pace for a wide range of subsequent geomorphic processes regardless of climate or lithology. Here, we employ the terms fracture and crack interchangeably to describe the open, low-aspect ratio discontinuities that result from mechanical weathering. Fracture propagation is widely understood to occur when stresses exceed the strength of rocks (e.g., Marder and Fineberg, 1996; Jaeger et al., 2009; Laubach et al., 2019). Rock fracture can further develop by stresses lower than the short-term strength of the rock, as localized strength is reduced due to chemical reactions, i.e., at subcritical stress levels (e.g., Griffith, 1921; Atkinson, 1987). Specifically, opening-mode subcritical cracking occurs when a fracture propagates under the condition of $K_I \leq K_{Ic}$ where K_I is the stress intensity factor and K_{Ic} is the mode-I fracture toughness (critical stress intensity) of the material (i.e., a material property; Atkinson, 1987). Such fracturing involves physico-chemical processes that include the breaking of chemical bonds weakened in response to localized stresses (e.g., Laubach et al., 2019) and/or chemical processes, such as chemical alteration, dissolution, and/or precipitation (e.g., Atkinson, 1982, 1984; Olson et al., 2009; Laubach et al., 2010; Rimsza et al., 2018). Subcritical cracking has been proposed by some researchers to dominate mechanical weathering (e.g., Walder and Hallet, 1985; Molnar, 2004; Stock et al., 2012; Eppes and Keanini, 2017; Eppes et al., 2018), because stresses that rocks experience at or near the surface of Earth are most commonly subcritical in magnitude (e.g., Walder and Hallet, 1985; Bost and Pouya, 2017; Collins and Stock, 2016; Jiménez-González et al., 2008; Martel, 2017; Ravaji et al., 2019). Yet direct field-based observations of fracturing evolution in natural surface environments through geologic time are scarce.

Open fractures develop in situ and subaerially within unconfined alluvial clasts in a wide variety of settings (e.g., Fig. 1). Here, we studied fractures in clasts perched on the top of late Quaternary terraces in the hyper-arid Negev desert in southern Israel (Figs. 1A and 2). To examine the evolution and characteristics of natural fractures in surface clasts we focused on fractures that were longer than 20 mm and partially traverse the clast without splitting it into two pieces, i.e., mode-I cracks that have not yet split the clast completely into two pieces (Fig. 3A). We employed petrographic, micro-chemical (scanning electron microscopy [SEM] mapping), and micron-scale roughness measurements to examine the morphology of natural fracture surfaces along their length from the rock surface inward, and compared them with the surfaces of fractures that we artificially and dynamically forced-open in the same sample with a chisel (hereinafter "forced-open fractures").

The results of the present work provide field-based evidence supporting the hypotheses that fracture propagation in surface rocks can occur progressively through geologic time and that water has a potential role in setting the rate of

Uri Shaanan https://orcid.org/0000-0003-1674-6184
Amit Mushkin https://orcid.org/0000-0002-5162-2550
Monica Rasmussen https://orcid.org/0000-0002-2816-0554
Amir Sagy https://orcid.org/0000-0002-6610-545X
Philip Meredith https://orcid.org/0000-0003-2193-5342
Yoshitaka Nara https://orcid.org/0000-0002-5717-1420
Russell Keanini https://orcid.org/0000-0002-7754-7907
Martha-Cary Eppes https://orcid.org/0000-0002-3032-1046
†urishaanan@gmail.com

GSA Bulletin;
published online 13 July 2023

https://doi.org/10.1130/B36670.1; 10 figures; 1 supplemental file.

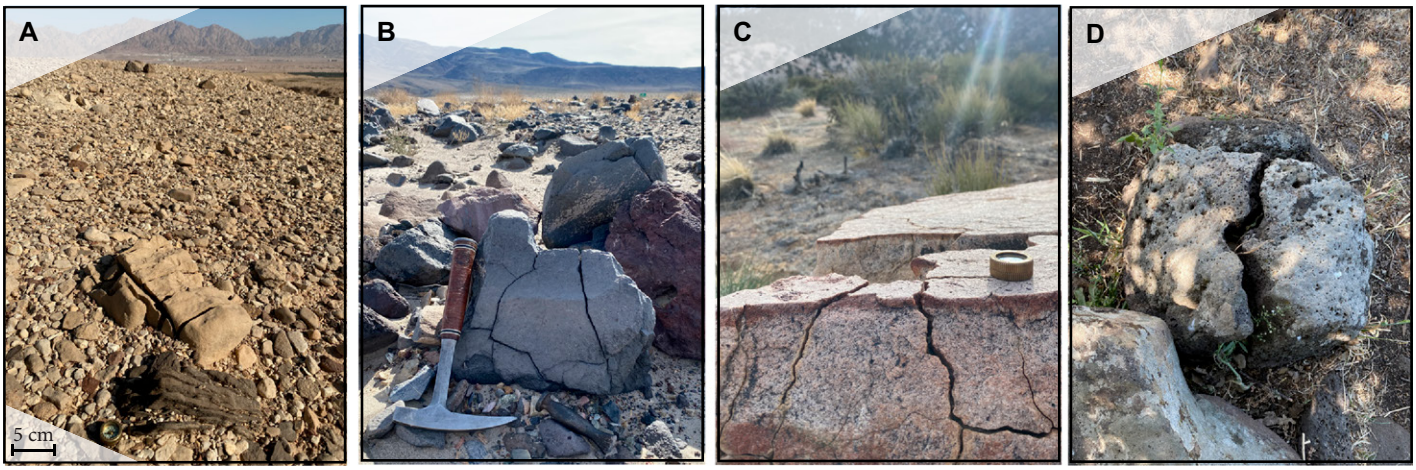

Figure 1. Fractured clasts on abandoned alluvial terraces. (A) Sandstone (dark) and micritic limestone (light) clasts on a 62 ka desert pavement, Shehoret fan, southern Israel. (B) Basalt boulder, Owens Valley, California, USA. (C) Granite boulder from Owens Valley. (D) Basalt boulder (50 cm in diameter) covered with lichen, northern Israel. Coin compass in panels A and C is 2.5 cm in diameter.

such fracture propagation as previously inferred from laboratory studies (Meredith and Atkinson, 1981, 1983; Atkinson, 1984; Nara and Kaneko, 2005; Nara et al., 2012, 2017; Chen et al., 2019, 2020), modeling (Eppes and Keanini, 2017), and direct field-based instrumental studies of subcritical cracking (Eppes et al., 2016, 2020). The study of the long-term history and controlling factors of near-surface fracture propagation has numerous implications for the understanding of subsequent surface processes and of the resilience of materials and structures.

APPROACH AND EXPERIMENTAL SETUP

To study how rocks fracture in subaerial settings and over geologic time scales we employed a space-for-time substitution approach and examined fractures in clasts deposited on a suite of co-genetic late Quaternary alluvial terraces of varying ages (Fig. 2), i.e., a "chronosequence." In arid environments such as the study area, where bioturbation and vegetation cover are minimal, desert pavements commonly start to develop on abandoned alluvial terraces within late Quaternary time scales (Cooke, 1970; Bull, 1977; Dan et al., 1982; Amit et al., 1993). Surface clasts on such pavements typically remain perched on the surface and experience continuous subaerial weathering (Wells et al., 1995; Mushkin et al., 2014). Thus, abandonment ages of desert alluvial surfaces (i.e., the time after which the sediment-supplying channel has migrated away, and weathering begins, and the surface is considered "stable") can be used as a first-order proxy for the overall duration of weathering (including fracturing) that clasts on the terrace surface have experienced (e.g., Mushkin et al., 2014). Accordingly, the present study builds on the previous approach of using alluvial chronosequences to study morphological "snapshots" of long-term, continuous surface maturation (weathering) processes (e.g., Stevens and Walker, 1970; Amit et al., 1993; Huggett, 1998; Mushkin et al., 2014; Hetz et al., 2016) to study fracture propagation in surface clasts over geologic time.

In the context of subaerial rock fracturing, the chronosequence approach also provides an effective "time 0" for fracturing activity because of the typically highly energetic transportation of alluvial clasts during desert flash floods (e.g., Greenbaum et al., 2020) to their current deposition on surfaces that ultimately stabilize as abandoned terraces. It is often assumed that any significant pre-existing weakness planes (e.g., inherited fractures) were most likely split during the alluvial transport, leaving only the more resilient or intact clasts or sections of clasts. This assumption is supported by field data showing positive correlations between transportation distance and rock strength (e.g., Olsen et al., 2020) and by the lack of well-developed fractures in clasts in the active stream channel (see "Fracture Number Density" section). Also, the fact that many of the clasts in desert pavements (and in the study site) occur as adjacent sections of a once-single clast (e.g., Fig. 1A) attests to the development of fractures in situ on the surface. Such clast configurations would not be possible to maintain during alluvial transport. Finally, the overall clast size decrease with surface age commonly observed on abandoned desert alluvial terraces (e.g., McFadden et al., 1989) and specifically at the study site of the present investigation (Amit et al., 1993; Mushkin et al., 2014) provides further evidence for in situ splitting of clasts on the surface. We posit that if the natural fractures formed dynamically, they should share common morphologic characteristics with the forced-open dynamic fractures, and their along-fracture morphology should not vary with distance from the rock surface.

Considering that the studied fractures formed in situ within non-confined clasts after their deposition on the alluvial surfaces, we can also assume that the primary stresses driving fracturing in such settings are neither tectonic, gravitational, or confining, but solely related to the surface environment. The hot, arid, and vegetation-free conditions (Fig. 1A), which have prevailed in the study area throughout the Quaternary (Amit et al., 2006), preclude stress loading by tree-related, brush-fire, or freezing processes. The latter requires both sufficient liquid water and extended freezing temperatures (Murton et al., 2006) that are not present at the study site. Accordingly, the primary plausible stresses we infer to be driving observed fracturing at the study site are most likely related to thermal cycling (e.g., McFadden et al., 2005; Eppes et al., 2016) and/or to salt weathering (Amit et al., 1993; Doehne, 2002).

In this work we assume that the fractures observed in the desert pavement clasts formed under generally low-magnitude stresses, such as those arising from solar oriented diurnal temperature variations. Such a fracturing mechanism has been shown in other works to result in preferred fracture strikes that correspond to the directional diurnal heating and cooling (McFadden et al., 2005; Eppes et al., 2010, 2015). Support for this working assumption is explained in the "Fracture Orientation" section in Methodology and Results sections.

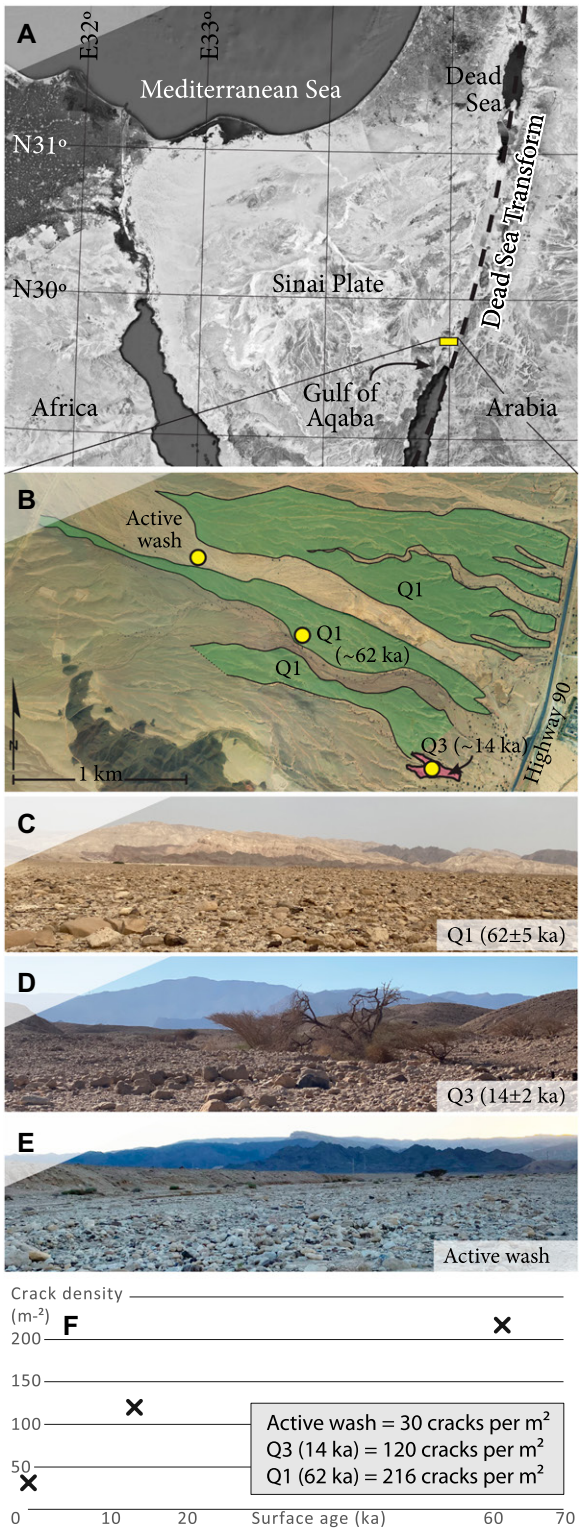

Figure 2. The study area and fracture number density measurements. (A) Satellite image of the region (Google Earth) and major tectonic/geographic elements. (B) Aerial photo of the study area with the alluvial surfaces that were examined and their ages (after Porat et al., 2010). Yellow circles denote the sites where fracture number density of 100 randomly selected clasts were measured. (C–E) Characteristic surface morphology of the studied alluvial surfaces (proximal clasts are fist to 50 cm in size). (F) Fracture number density measurements from the Shehoret alluvial fan (see Table S1 for comprehensive list of data [see text footnote 1]). Site coordinates: Active wash: 29°37′0.99″N/34°57′47.09″E; Q3: 29°36′21.26″N/34°58′37.58″E; Q1: 29°36′49.46″N/34°58′7.79″E (WGS84).

STUDY AREA AND METHODOLOGY

Study Area

The Shehoret alluvial fan is located within the Arava Valley segment of the Dead Sea Rift Valley (Israel), ~7 km north of the Gulf of Aqaba (Fig. 2A). Bedrock exposures in the catchment of the fan include crystalline basement outcrops of the Neoproterozoic Arabian-Nubian Shield as well as overlying Cambrian sandstones and Phanerozoic carbonate rocks (Beyth et al., 2012). Tectonic subsidence of the valley floor, associated with activity along the Dead Sea Transform (Fig. 2A), has led to base-level lowering and stepwise abandonment of alluvial terraces. These abandoned terraces all share common lithological, depositional, and climatic settings and thus form a sequence of distinct morpho-stratigraphic units, i.e., an alluvial chronosequence, which was previously studied as a type-location for reg soil (petrogypsids, aridisols) and desert pavement development (Amit et al., 1993, 1996). Exceptional age control for abandonment of multiple late Quaternary terraces at Shehoret (Porat et al., 2010) has previously facilitated quantitative studies of subaerial rock fragmentation through the late Quaternary at this specific site (Mushkin et al., 2014). In the present study, we focused primarily on surface clasts in the active wash (assumed to represent "time 0") and on desert pavements capping Pleistocene terraces Q1 and Q3, previously dated to 62 ± 5 ka and 14 ± 2 ka, respectively (Fig. 2B; Porat et al., 2010).

The lithology of Shehoret fan terraces is dominated by carbonates, with felsic magmatic rocks and sandstones occurring to a lesser degree. The carbonate clasts are namely micritic limestones, characterized by epigenetic dolomitization (i.e., partial alteration of Ca with Mg), which appears as rhombohedral dolomite [$(Ca,Mg)CO_3$] crystals in a fine limestone [$CaCO_3$] matrix (see Petrography section). The climate in this region has been hyper-arid and stable throughout the Quaternary (Amit et al., 2006). Annual rainfall is presently under ~60 mm (Barzilai et al., 2000) with significant clast-mobilizing flash floods occurring roughly every 2–3 years. Aeolian dust and salts are common in the region and accumulate in the soil section beneath the desert pavement (Amit and Gerson, 1986; Ben-Israel et al., 2015; Crouvi et al., 2018). Terrace abandonment ages in the study area are well-constrained from past studies (Porat et al., 2010) and soil characteristics provide strong evidence that Q1 and Q3 surfaces have neither been eroded nor buried since their abandonment (Amit et al., 1993). Namely, clasts presently perched on these surfaces have been continuously exposed since the time of their deposition.

Methodology—Field Observations

Fracture Number Density

To document fracture distribution in the Shehoret surface clasts, we counted the visible fractures on 100 individual clasts from the active wash (i.e., time 0), the Q3 (14 ± 2 ka) terrace, and the Q1 (62 ± 5 ka) terrace (Figs. 2B–2E, 300 clasts all together). Alluvial clasts meeting

a size criterion of 5–50 cm in diameter were selected at ~1 m intervals based on the closest proximity to a measuring tape extended across the terrace (oblique to the paleo-flow-direction). Recorded parameters for each clast included length, width, height, burial depth, lithology, and the number of visible fractures longer than 20 mm (see results and Table S1[1]). Fracture number density was then calculated for each terrace separately as the total number of fractures normalized to the total surface area of clasts (Fig. 2F). We note that fracture number densities calculated herein from the field-based fracture/rock counts should be regarded as minimum bounds because they cannot account for fully developed fractures that have already split clasts into separate pieces.

Fracture Orientation

A large body of prior work on the orientations (strike and dip directions) of fractures measured in surface clasts on stable surfaces similar to those examined in the present study shows that such fractures often exhibit statistically preferred orientations (McFadden et al., 2005; Adelsberger and Smith, 2009; Eppes et al., 2010; D'Arcy et al., 2015; Aldred et al., 2016). These orientations are commonly interpreted to arise due to the directionality of peak diurnal thermal stresses that occur due to the east-west transit of the sun across the sky (e.g., McFadden et al., 2005). To support our working assumption that fractures observed in the present study formed under generally low-magnitude stresses, such as those arising from diurnal temperature variations, strike measurements were collected from a subset of 100 different 5–50 cm clasts containing three or more subparallel fractures with verging opposing surfaces that are consistent with each other, implying that they preserve the original in situ fracture strike (e.g., Fig. 1A).

Fracture-Surface Morphology

We recorded fractures on exposed surfaces that had only partially split clasts and were visible on the upward facing surface of the clast. In total, we examined over 500 of these fractures, primarily from the Q1 surface, by forcing them open with a chisel. The chisel was placed at the fracture opening aligned with its long axis, so that upon impact the pre-existing fracture was extended and the clast was completely split so that the original fracture surface could be examined (Figs. 3A and 3B). The surfaces of the natural portions of the fractures were then examined and also compared with those of the forced-opened portions of the fractures.

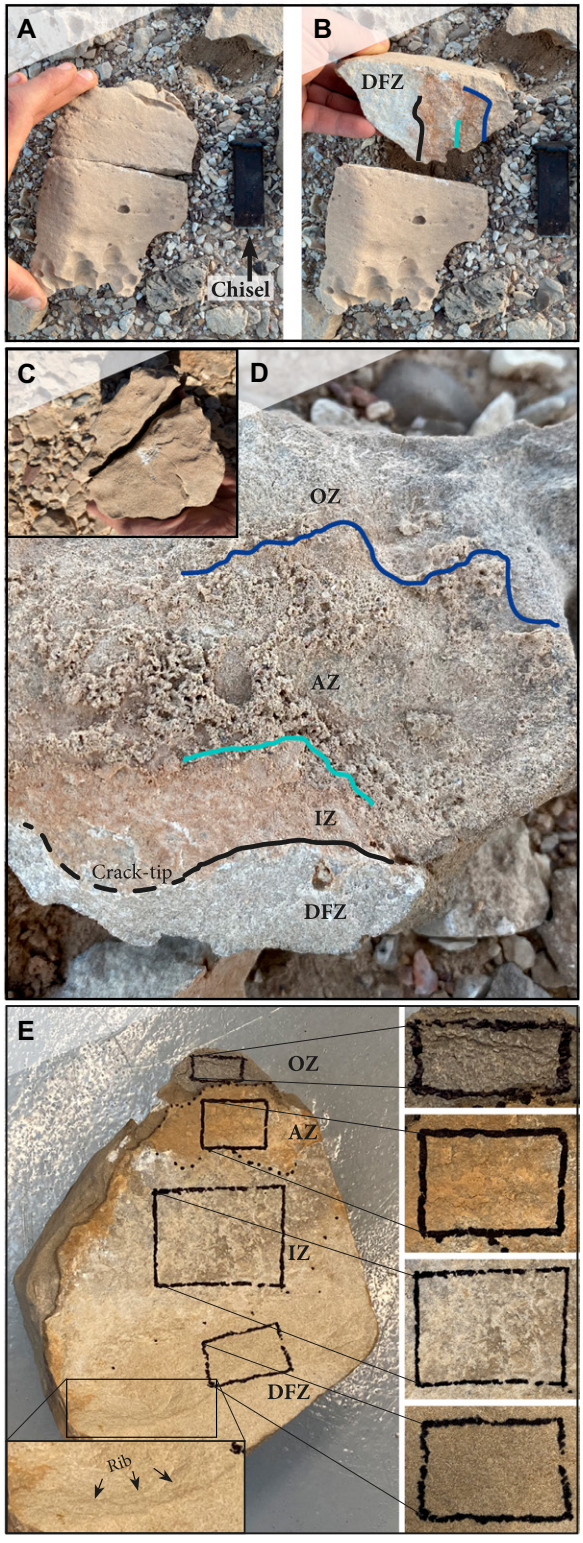

Figure 3. Typical mesoscopic-scale zonation within the examined fractures in micritic limestone clasts from the Shehoret fan, southern Israel. (A) Fracture before being force-opened. (B) Force-opened fracture surface with zonation boundaries annotated. (C and D) Fist-size clast (C) and exposed fracture surface (D, not washed). (E) Force-opened fracture surface after being washed (clast is ~20 cm long). OZ—Outer Zone; AZ—Accumulation Zone; IZ—Inner Zone; DFZ—Dynamic Fracture Zone. Dark chisel (8 cm) used for force-opening the fracture.

Methodology—Lab Observations

Petrographic and SEM Analyses

Optical (polarizing light) and SEM (FEI Quanta 450, with INCA software) analyses of fracture surfaces were conducted at the Geologi-

[1]Supplemental Material. Table S1. Fracture number density measurements (XLS spreadsheet). Figure S1. Fracture strike data (PDF). Supplemental Data S1. Roughness analyses (data—3-D scans as referenced images). Please visit https://doi.org/10.1130/GSAB.S.22669468 to access the supplemental material, and contact editing@geosociety.org with any questions.

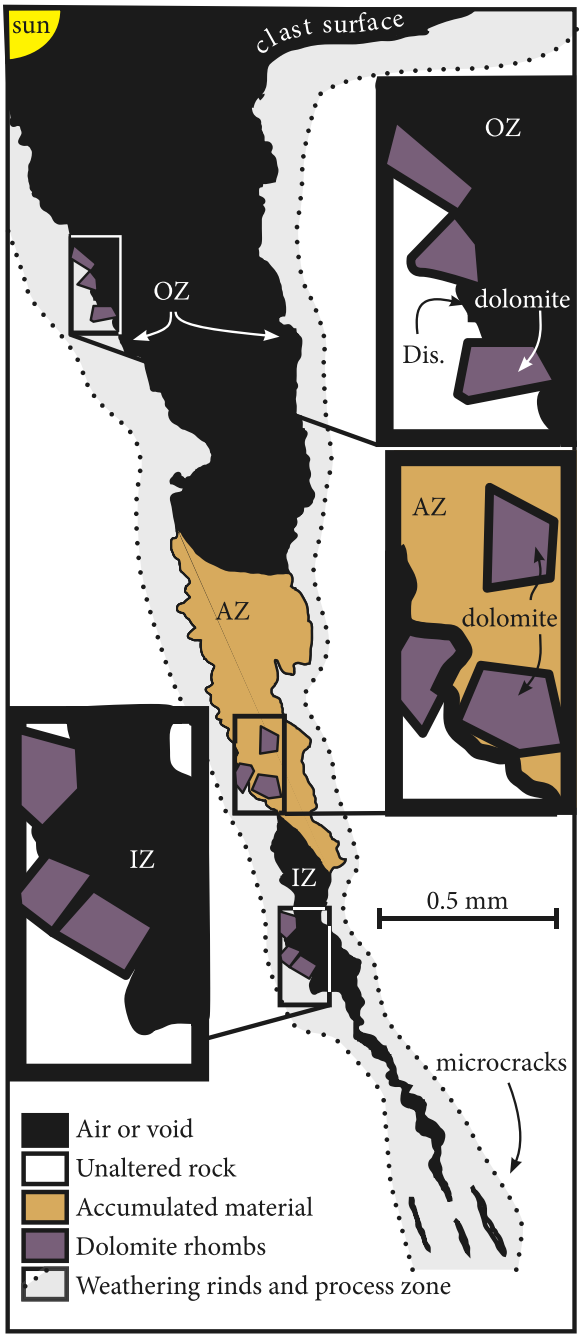

Figure 4. Diagram of fracture morphology illustrating characteristic fracture zonation, sketched over photomicrographs from sample 178_SH_sh from the Shehoret fan, southern Israel. Black is fracture void, brown is accumulated material within the Accumulation Zone, purple-gray is dolomite rhombs (illustrated within the area of insets but occurring throughout), and the dotted line denotes an estimated process zone. OZ—Outer Zone; AZ—Accumulation Zone; IZ—Inner Zone; Dis.—dissolution morphology.

cal Survey of Israel, Jerusalem, Israel. To inspect fracture surface morphology and composition, opened fracture surfaces were thoroughly rinsed with water. Thin sections normal to fracture surfaces were cut after impregnation of open fractures with epoxy resin. These "fracture-normal" thin sections extend into the host rock beyond the crack-tip. Photomicrographs were collaged using Adobe InDesign software.

Roughness Analyses

Two-dimensional roughness analysis was conducted on a high-resolution collage of photomicrographs from a thin section oriented perpendicular to the surface of the fracture. The high-resolution collage extends along the entire surface of the fracture from the outer rim of the clast and into the non-deformed rock beyond the crack-tip. The traces of fracture surfaces were digitized as the boundary between the rock and the epoxy filling and/or voids, and the equation used is similar to that used for the 3-D analysis described in the next paragraph.

Three-dimensional roughness analyses of fracture surfaces were conducted using microtopographic digital elevation models (DEMs) produced at 10-micron resolution using an "Opimet Conoscan-10" 3-D laser profilometer at the Geological Survey of Israel (See Morad et al., 2022, for scanning procedure and details). Surface roughness was quantified using root mean squared deviation (RMSD) values calculated as:

$$RMSD_{(L)} = \sqrt{\frac{\sum_{i=1}^{N_{(L)}} \left(z_i - \hat{z}_i\right)^2}{N_{(L)}}} \qquad (1)$$

where L is the length of the profile interrogated, z is the measured elevation at pixel i, $\hat{z}$ is the modeled elevation for a linear regression across L, and N is the number of pixels along the interrogated profile L. The RMSD of profiles in the x and y direction (distance of scanned pixels on horizontal grid) was examined to verify that there was no anisotropy for roughness. Reported RMSD values are averages for all parallel profiles in both the x and y directions of the DEM.

RESULTS

Fracture Number Density

Fracture number density in the Shehoret clasts increased by an order of magnitude within late Quaternary time scales (Fig. 2F): The baseline ("time 0") data set obtained from 100 clasts in the present-day active Shehoret wash yielded a mean fracture number density of 30 fractures per square meter, with an average of 0.3 fractures per clast. Fracture number densities on the Q3 (14 ka) and Q1 (62 ka) terraces were 118 and 215 fractures per square meter, respectively (Table S1), with averages of 0.6 and 1.4 fractures per clast, respectively (see Table S1 for complete data).

Fracture Zonation and Morphology

Field examination of the observed fractures in the fully split clasts from the Q1 and Q3 surfaces revealed a recurring pattern of three naturally occurring zones (areas of the fracture surfaces and filling/void between them) of distinct weathering characteristics extending from the clast exterior toward the clast interior and crack-tip (Figs. 3 and 4).

(1) The "Outer Zone" extends several centimeters inward from the clast surface. This zone has a similar color and morphology to the upper surface of the clast exterior and is characterized by a sandstone-like "sugary" texture and weathering rind (i.e., patina or oxidation, coating or recrystallization in the external millimeters that are most exposed to surface conditions). The rims of the fracture opening where they intersect the

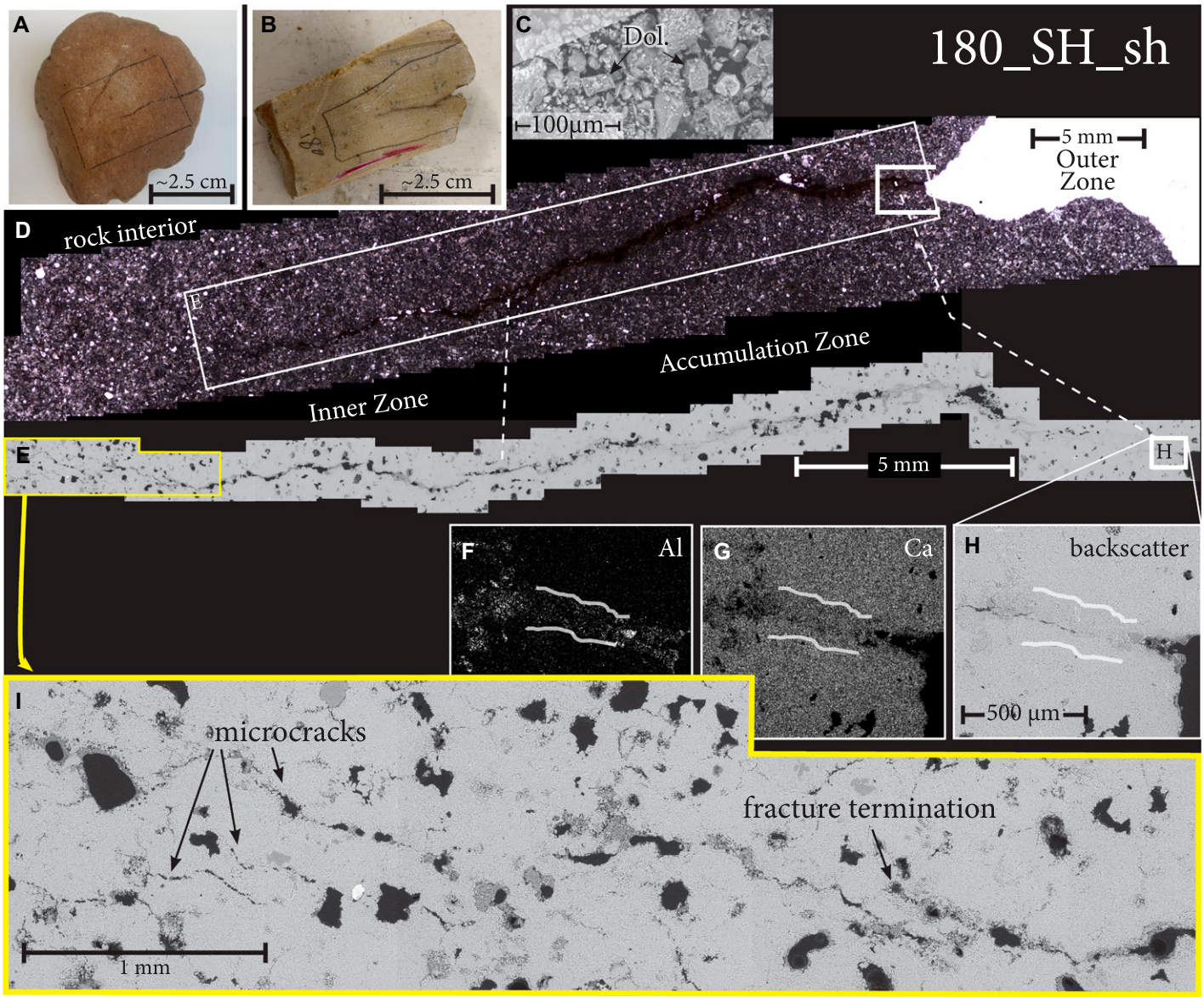

Figure 5. Sample 180_SH_sh, from the Q1 (62 ka) alluvial terrace of the Shehoret fan, southern Israel. (A) Hand sample with fracture. (B) Sawed sample, after impregnation with epoxy, perpendicular to the fracture surface. Pencil marking denotes the area of the thin section. (C) Parallel polarizing light photomicrograph of the material accumulated in the Accumulation Zone, containing loose dolomite rhombohedral crystals (Dol). (D) Collage (75 images) taken in parallel polarizing light through the entire fracture. (E) Collage of scanning electron microscope (SEM) backscatter electron images of the fracture (22 images) and its termination. (F and G) SEM chemical mapping of aluminum and calcium, respectively, of the area photographed by backscatter electron in panel H (marked by white rectangle on panels D and E). The area constrained by white strokes in panels F and G denotes visible change in the distribution of aluminum and calcium, respectively (and corresponding boundaries on the backscatter image, i.e., panel H). (I) Enlargement of the area where the fracture terminates and microcracks are visible ahead of the crack-tip in the process zone (four images).

outer surface of the clast are generally rounded, suggesting significant weathering. The surface of the fracture Outer Zone was consistently rougher and darker than that freshly exposed in force-opened fractures in the same clast (Fig. 3E).

The exterior of all the dolomitized micritic limestone clasts on the Q1 surface was characterized by a well-developed sugary patina (Amit et al., 1993). Clasts of the same lithology on the younger Q3 surface displayed a less developed patina in contrast, while a patina is mostly absent in clasts of the active wash.

(2) The "Accumulation Zone" that extends farther inward from the Outer Zone and is characterized by an amalgamation of fine-grained particles that fill the void between the two opposing surfaces of the fracture (fracture filling). Petrographic and SEM analysis revealed that this accumulated material consists of quartz, clay, and other particles that are not present in the examined carbonate clasts. These materials are likely sourced from aeolian dust. In addition, loose dolomite rhombs likely sourced from the fracture surfaces were

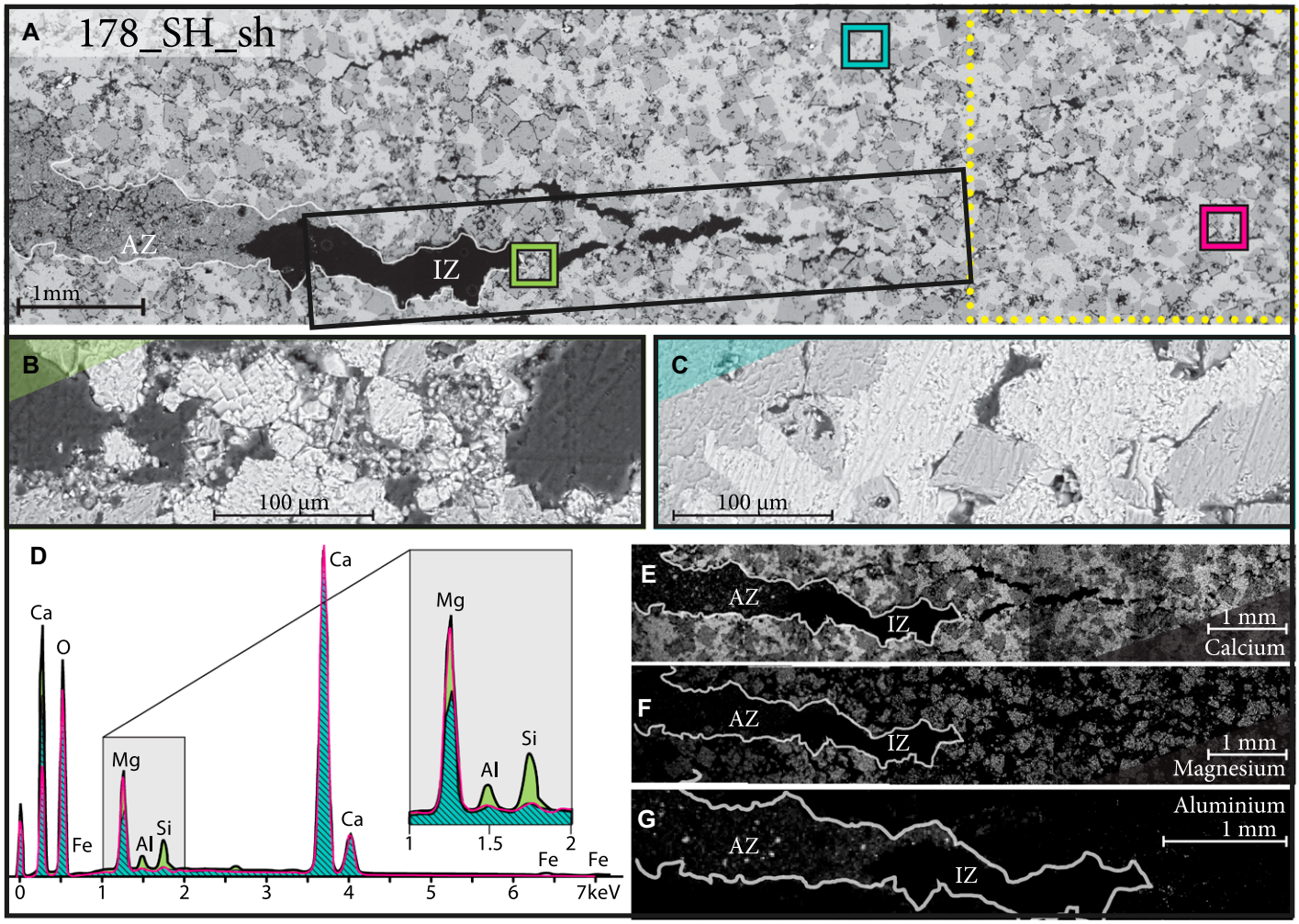

Figure 6. Scanning electron microscope (SEM) results for sample 178_SH_sh from the Q1 (62 ka) terrace of the Shehoret fan, southern Israel. (A–C) Backscatter electron images of the fracture with insets B and C taken on and away from the fracture, respectively, on sections from the areas denoted in green and cyan, where chemical mapping presented in panel D were conducted. Dotted yellow box in panel A denotes the area where deformation terminates. (D) SEM elemental map of areas in the Inner Zone (green), the host rock (cyan), and beyond the crack-tip (pink). (E–G) SEM elemental mapping of calcium (E), magnesium (F), and aluminum (G). AZ—Accumulation Zone; IZ—Inner Zone.

found in the accumulated material (Figs. 4 and 5C). Soluble salts are notably absent in these infilling materials. Brushing and/or rinsing the loose material from the fracture surfaces revealed a brownish-reddish iron-oxide staining on the fracture surface that could be readily distinguished from the surface of the Outer Zone (Fig. 3E). The fracture aperture along the Accumulation Zone is generally smaller than that of the fracture along the Outer Zone, and larger than the fracture aperture along the "Inner Zone" such that fracture aperture and overall width generally decrease with increasing distance from the clast surface.

(3) The "Inner Zone" extends inward from the Accumulation Zone to the crack-tip and is void of loose particles. The Inner Zone also decreases in aperture toward the crack-tip-line. The surface of the Inner Zone is stained with reddish oxides, but typically at a lesser intensity than that observed along the Accumulation Zone (Figs. 3B and 3E).

We also refer to an additional "zone" that we created in the clasts by forcing fractures open with a chisel; these artificially induced surfaces extend beyond the tip of the natural fracture. These artificially induced fresh fracture surfaces provide an opportunity to examine the surface morphology of dynamically opened fractures in the examined sample and therefore are referred to as a "Dynamic Fracture Zone" (DFZ). The surfaces of the DFZ were characteristically orientated at approximately a 30-degree angle relative to the trend of the pre-existing fracture. The surfaces of DFZs contained evidence of plumose textures and associated ribs (Fig. 3E), whereas no such features were observed along the three zones of the natural fractures.

Petrography

About 30 representative dolomitized micritic limestone clasts from the Q1 terrace with fractures that did not completely split the clast were examined in the lab. Optical petrography (data from 5 thin sections) confirmed that the selected rocks were micritic limestone clasts that experienced epigenetic dolomitization resulting in the pervasive occurrence of euhedral to subhedral dolomite rhombohedrons homogeneously distributed throughout the microcrystalline calcium carbonate matrix (e.g., Gregg and Sibley, 1984) (Figs. 6A and 6C). The uniformity and homogeneous distribution of dolomite rhombs indicate that dolomitization occurred within the source bedrock prior to detachment and subsequent alluvial transport. The petrographic observations also

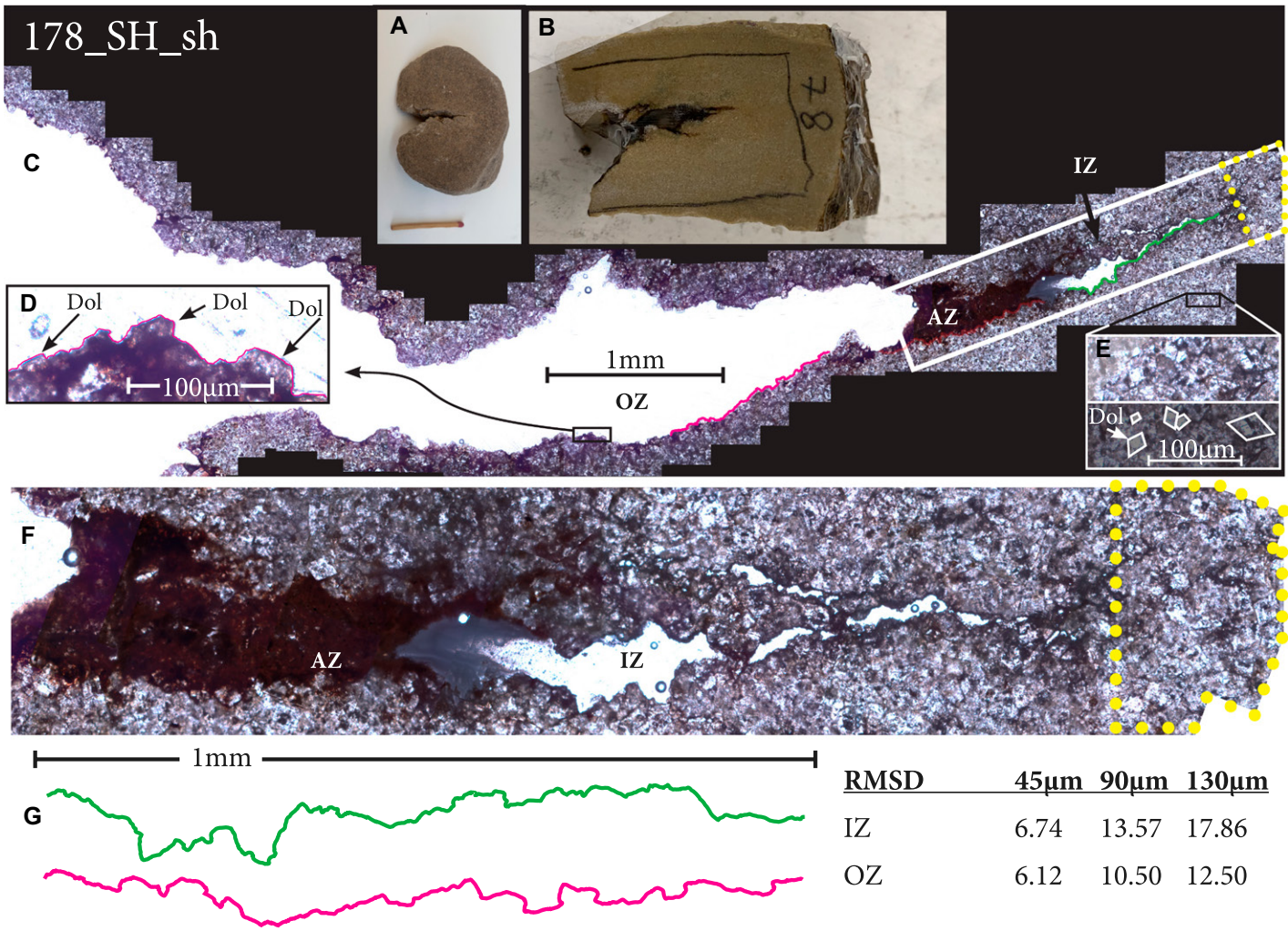

Figure 7. Fracture in sample 178_SH_sh taken from the Q1 (62 ka) alluvial terrace of the Shehoret fan, southern Israel. (A) Hand sample (with a standard match for scale). (B) Same sample, after impregnation of the fracture with epoxy, and perpendicularly sawed fracture surface. Pencil marking denotes the area of the thin section displayed in panels C–F. (C) Photomicrograph collage (94 images) taken with polarizing light. (D) An inset from the Outer Zone with black arrows denoting dolomite rhombs (Dol). (E) High-magnification image of the host rock away from the fracture surface, without (top) and with (bottom) annotation of dolomite rhombohedral crystals. (F) An inset of the Accumulation Zone and Inner Zone of the fracture (for scale see inset size in panel C). Dotted yellow marking denotes the area of the rock where deformation terminates beyond the crack-tip. (G) Roughness analyses for representative sections of the Outer, Accumulation, and Inner zones, at 45, 90, and 130 µm length scales, respectively, as marked on panel C. OZ—Outer Zone; AZ—Accumulation Zone; IZ—Inner Zone; RMSD—root mean squared deviation.

indicated that the clast interiors beyond the crack-tip do not generally display any apparent weakness planes such as bedding, foliation, or micro-veins.

Petrographic analysis also revealed that the sandstone-like "sugary" texture of the Outer Zone is likely associated with the characteristic 10–200 µm size of the dolomite rhombs embedded in the micritic $CaCO_3$ matrix, which appears to be more susceptible to weathering (Fig. 7D). The presence of loose dolomite rhombs within the Accumulation Zone material (Fig. 5C) supports preferential dissolution of the $CaCO_3$ matrix relative to the dolomite rhombs.

Scanning Electron Microscopy (SEM)

SEM analyses confirmed the predominately micritic limestone ($CaCO_3$) composition of the matrix and the dolomitic ($[Ca,Mg]CO_3$) composition of the rhombs (Fig. 6D). Backscatter electron images denote the dolomite rhombs as darker gray polygons and their distribution to be uniform throughout the rock (Figs. 6A and 6C).

Elemental mapping in the SEM confirmed that the loose material in the Accumulation Zone contained allochthonous elements that are absent in the observed dolomite clast such as aluminum, silicon, and iron (some, at least, as oxides). Furthermore, examination of the rock interior adjacent to the fracture along the Outer, Accumulation, and Inner zones revealed weathering rinds of these "foreign" elements that penetrate into the $[Ca,Mg]CO_3$ host rock whereas calcium abundance is depleted (Figs. 6D, 8D, and 8F).

The backscatter electron and the petrographic images (Figs. 6A, 7C, and 7F, respectively), reveal that natural fractures propagated intergranularly, largely along rhomb boundaries. At the inner tip of the Inner Zone the fracture appears to terminate gradually with deformation beyond the tip of the fracture dispersed as small elongated voids (hereinafter

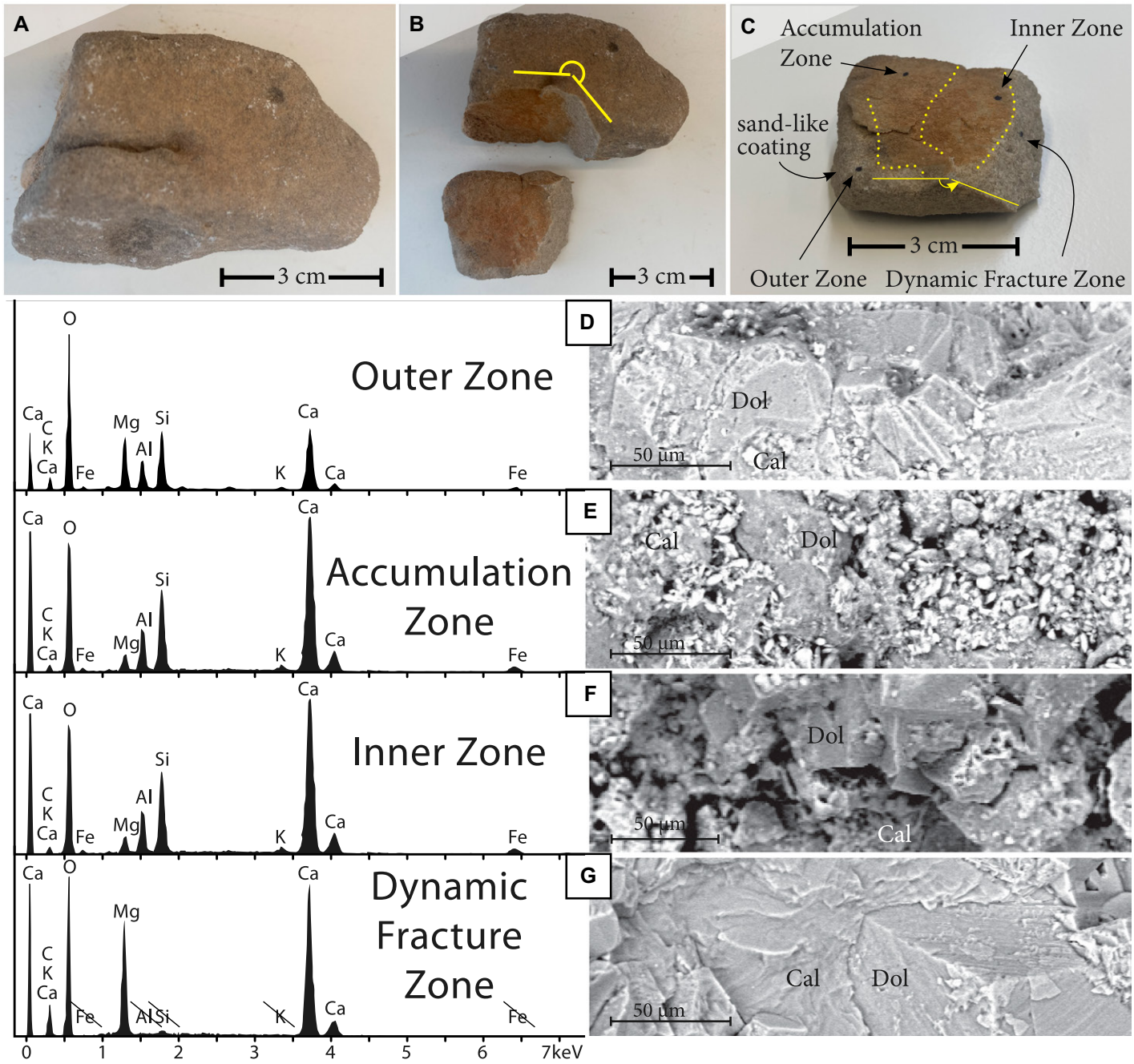

Figure 8. Scanning electron microscope (SEM) examination of the fractured zone surfaces from a specimen of the 62 ka terrace of the Shehoret fan, southern Israel. (A) Hand sample. (B) The forced-open fracture photographed in panel A with the top piece in same orientation as in panel A. Note the annotation for the different orientations of the fracture and the forced dynamic fracture. (C) The examined section of the clast photographed in panel A and bottom of panel B, with annotation for zonation boundaries and ink points marking the SEM sites of analyses and images presented in panels D–G (marked after analyses concluded). (D–G) SEM chemical results of spot-analyses for the micritic limestone matrix (not the dolomite crystals), and corresponding backscatter electron images of the analyzed surface. Cal—calcium; Dol—dolomite.

"microcracks") that diminish in abundance with distance from the tip (Figs. 5I and 6A). The microcracks ahead of the crack-tip are aligned with the direction of the natural fracture and comprise a "process zone" that is not yet fully connected to the opened section of the fracture (Figs. 5I and 6A). SEM elemental mapping revealed allochthonous elements within this process zone (Fig. 6D). In the vicinity of the fractures, no evidence such as aligned minerals, bedding planes, or veins were observed (e.g., Figs. 5D, 5I, and 6A) that would suggest pre-existing inherited weakness planes in the "undeformed" rock that may dictate the orientation of fracture propagation. SEM backscatter images show that the surfaces of the Outer, Accumulation, and Inner zones contain 5–100 µm wide voids that occur between the dolomite rhombs (Figs. 8D–8F). These voids are largely absent in the freshly exposed Dynamic Fracture Zone (Figs. 8G and 9B).

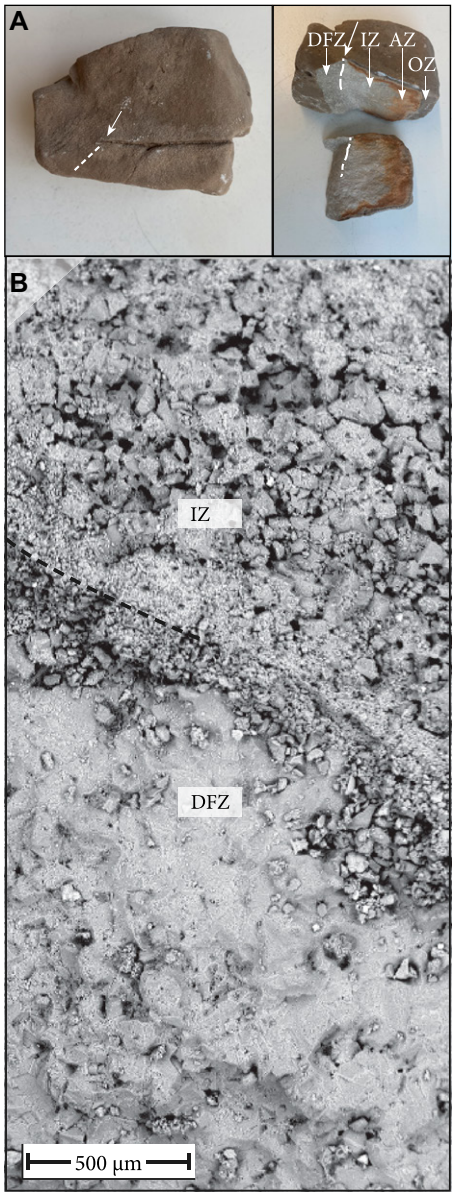

Figure 9. Fracture tip morphology (from a specimen of the 62 ka terrace) of the Shehoret fan, southern Israel. (A) Photographs of a fist-size clast (5 cm in diameter) with its crack-tip annotated before (left) and after (right) forced-opening with a chisel. Note the different orientation of the dynamic fracture (i.e., Dynamic Fracture Zone, DFZ) in respect to the previously existing subcritical crack (i.e., Outer, Accumulation, and Inner zones; OZ, AZ, and IZ, respectively). (B) Scanning electron microscope image of the fracture surface just located at the tip of the natural fracture displayed in panel A (denoted by dashed stroke). The DFZ looks smooth because it has cut through rhombs, reflective of fast fracture (artificially made in this study), and the contrasting rough IZ surface reflects intergranular fracture, indicative of slow, subcritical cracking. Karst-like micro morphology and development of voids up to the fracture edge suggest dissolution and water activity at or up to the crack-tip. Dolomite rhombs are primary features of the clast.

Roughness Analysis

Two-dimensional roughness analyses conducted on a representative thin section (Fig. 7G) revealed that the Inner Zone surface was rougher than that of the Outer Zone. The examined thin section consists of 10–50 μm dolomite rhombs and thus RMSD values of the fracture profiles were calculated at length scales of 45, 90, and 130 μm, which correspond (i.e., are sensitive) to the rhomb length-scale. For all length scales, Inner Zone RMSD values were higher (rougher) than those of the Outer Zone. RMSD values for the Accumulation Zone are not presented due to low certainty and difficulties in accurately determining the boundary between rock and loose material along the Accumulation Zone (Fig. 7).

Roughness analyses for representative surfaces (3-D analyses) of the Outer, Inner, and Dynamic Fracture zones revealed that RMSD values monotonically increased with length scale for all the examined zones (Fig. 10). The Inner Zone was consistently rougher than the Outer Zone at all measured roughness scales. The Inner Zone also consisted of rhomb-shaped protrusions and cavities (likely associated with individual dolomite rhombs), which are less apparent along the smoother surface of the Outer Zone (Figs. 10B and 10D). At length scales above 150 μm the Dynamic Fracture Zone is smoother than the Inner Zone. See Supplemental Data S1 for roughness data.

Fracture Orientations

The fracture strikes measured at Shehoret display a preferred WNW-ESE directionality (Fig. S1). This observation is in line with published fracture orientation data for similarly stable surfaces where subaerial fracturing was previously linked to diurnal variations in thermal stress (McFadden et al., 2005; Eppes et al., 2010, 2015).

DISCUSSION

Evidence for Progressive Fracturing over Geologic Time

The observed positive correlation between inferred clast exposure ages and fracture number density on the late Quaternary Shehoret chronosequence surfaces (Fig. 2F) indicates that the fractures developed in situ as they increased in number over geologic time. If fractures were inherited from pre-deposition time, then this correlation, or the occurrence of fully split clasts with adjacent sections in their relative position (e.g., Fig. 1A), would be less likely. We find several independent lines of evidence that point toward progressive propagation of individual fractures. This progression may occur as continuous subcritical cracking, as incremental steps of dynamic fracture, or incremental periods of subcritical fracture. It is not possible to confidently distinguish between these possibilities from our current data set. With that in mind, our data are supportive overall of progressive fracturing as opposed to the dynamic, instantaneous rupture of the entire fracture.

First, the overall decreasing degree of weathering from the Outer to Inner zones suggests sufficient differences in exposure time of these portions of the fractures to weathering processes. For example, oxide coatings like those observed in the fractures are a common secondary weathering feature in desert pavement clasts and are known to get darker and redder with increasing exposure age (e.g., McFadden et al., 1989). For the fractures examined herein, coating along the Inner Zone was commonly less intense than that along the Outer Zone. We interpret these differences as reflecting a longer exposure time for Outer Zone relative to the Inner Zone such that the oxidation differences could develop, acknowledging that they could form as a fracture-depth dependent feature.

Additionally, the sugary texture found along the Outer Zone, which resembles that found on the clast exterior, is largely absent or less developed along the Accumulation and Inner zones (Figs. 3B, 3D, 3E, 7G, and 10). There is, however, an increase in roughness between the Outer and Inner zones along the fracture length (Fig. 7G). We suggest that this difference in texture is caused by preferential dissolution of calcite matrix after fracturing has occurred, and that this process leads to time-dependent smoothing of the different fracture zones over geologic time. The differences in apparent degree of dissolution could also conceivably be attributed to changes in water chemistry as a function of distance along the fracture (McFadden et al., 1998). However, at Shehoret we observed no evidence for this, such as carbonate coatings that would be suggestive of a switch from carbonate dissolution to precipitation conditions along the fracture. Similarly, the differences in weathering between the Outer and Inner zones could also occur if the fractures formed at once, but then their outer zone experienced more intense

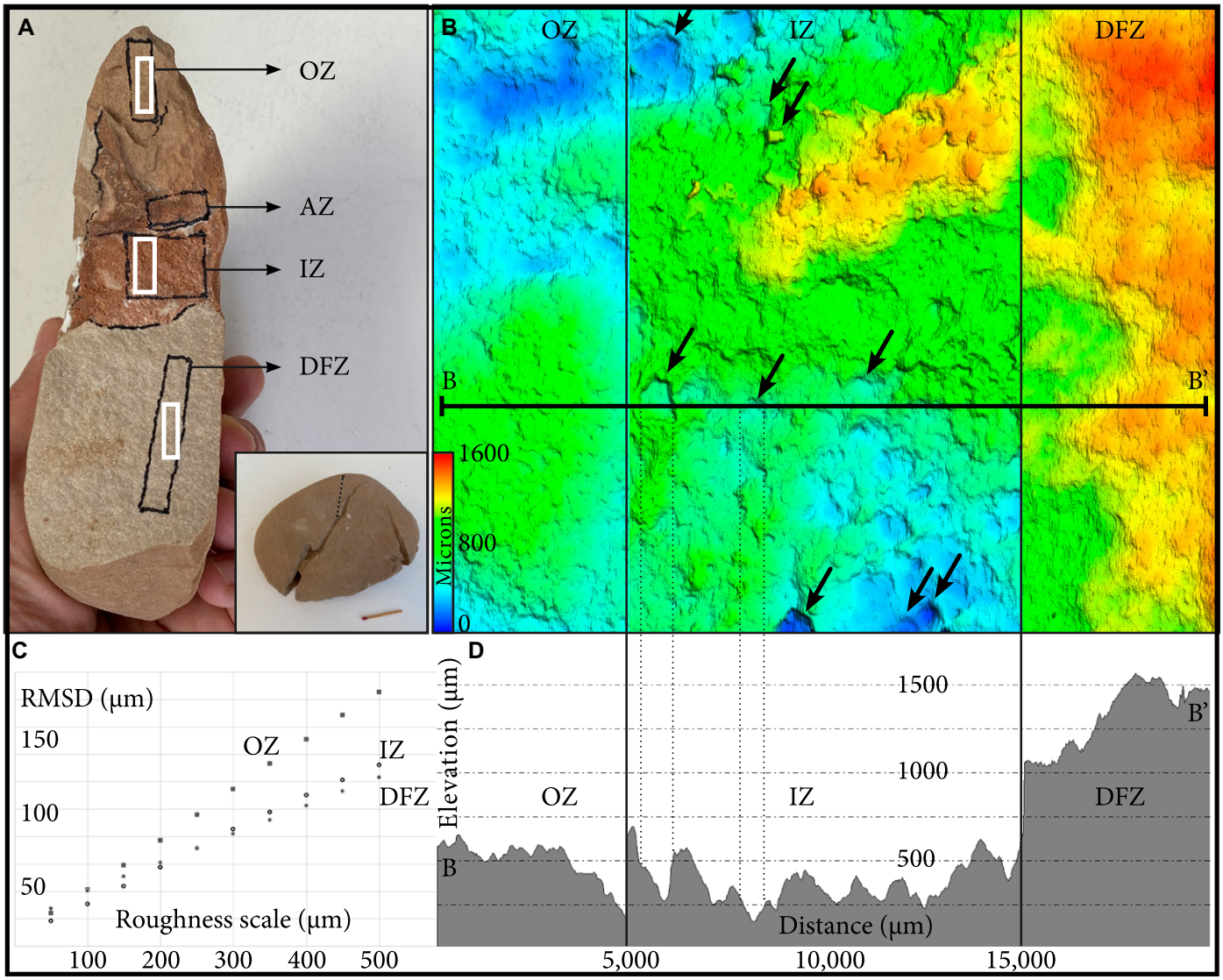

Figure 10. Fracture 3-D roughness measured with a laser profilometer. (A) Hand sample 187_SH_sh (Shehoret fan, southern Israel), showing the three characteristic weathering zones of observed fractures (Outer, Accumulation, and Inner zones; OZ, AZ, and IZ, respectively) and the Dynamic Fracture Zone (DFZ). Inset at bottom right shows the clast before forcing-open, with a match for scale and annotation for the orientation of the DFZ. White boxes mark the scanned areas displayed in panel B. (B) Micro-topography along the OZ, IZ, and DFZ (AZ not shown). Black arrows highlight dolomite rhombs and rhomb ghosts. (C) Spectral roughness of the fracture zones, illustrated through root mean squared deviation (RMSD) measurements at multiple length scales. (D) Cross section B–B′ (projected from panel B), illustrates roughness differences between the fracture zones. See Supplemental Data S1 for source data (see text footnote 1).

weathering conditions closer to the clast exterior. However, the continued increase in fracture number density during the late Quaternary (Fig. 2F) argues against a single pulse of fracture growth.

In addition to the differences in the degree of weathering along the natural fracture traces, fracture surface morphology appears more consistent with progressive fracturing rather than instantaneous rupture along the entire fracture length. Experimental fracture mechanics observations suggest that dynamic versus progressive fracturing can result in different fracture surface morphologies. Dynamic fracture propagation typically results in fracture pathways that are quasi-planar and/or branching (e.g., Lawn and Wilshaw, 1975). Fractures that propagate rapidly and unstably tend to crosscut individual grains and other heterogeneities (Barnett and Kerrich, 1980). In addition, dynamic fracturing is known to produce typical morphologies such as plume structures or sub-parallel ribs. We find all of these characteristics along the artificially formed surfaces which were produced dynamically (the Dynamic Fracture Zone) (Figs. 3E and 9B). In contrast, the micro-morphological attributes of the natural portions of the fracture surfaces are distinctly different. Specifically, our results demonstrate the intergranular nature of the natural fracture pathways along all the natural zones of the fractures. Both the Inner Zone and the microcracks that are situated ahead of the crack-tip preserve dolomite rhomb crystal morphologies that point toward fracture propagation along grain (rhomb) boundaries (Figs. 5I and 10B). Such structures are consistent with laboratory observations of slow-paced or stable subcritical crack growth (Barnett and Kerrich, 1980; Kerrich et al., 1981; Swanson, 1984; Kudo

et al.,1992; Nara et al., 2006). When cracking propagates subcritically, fracture pathways commonly follow grain boundaries that typically link microcracks ahead of the crack-tip (e.g., Kerrich et al., 1981; Swanson,1984; Kudo et al.,1992; Nara et al., 2006; Voigtländer et al., 2018). We thus propose that the observed intergranular morphology of the Inner Zone fracture surfaces and that of the microcracks ahead of the crack-tip are consistent with subcritical propagation of the natural fractures in the Shehoret clasts. Alternatively, the intergranular topography of the fracture surfaces (as well as the decreasing weathering along the length of the fracture) that we observed may represent short pulses of fracture (either critical or subcritical) and more data and work are needed to confidently rule out such a process. However, the overall fracture history appears to be progressive rather than a single discrete fracturing event.

Finally, the inferred driving stresses of the fractures in the Shehoret clasts are also generally consistent with a dominance of subcritical crack propagation. Because the observed fractures are found in randomly deposited clasts with no signs of apparent weakness planes such as bedding, foliation, or micro-veins parallel to most fractures, and the fact that some clasts are fully split with segments embedded in place imply that these occurred in situ by post-depositional stresses. Solar induced directional insolation is one likely generating force. This mechanism generates diurnal thermal fluctuation that is anisotropic as it is sourced from the sun and therefore acts differently on surfaces with different orientations. The observed preferred WNW-ESE strikes of fractures in the study area (Fig. S1) point toward post-depositional directional insolation as a significant driving force of these fractures (e.g., McFadden et al., 2005; Eppes et al., 2010, 2015; Aldred et al., 2016). Numerical modeling for clasts of the size of those in this study suggests that such whole-rock stresses are generally low in magnitude (e.g., $<$0.8 MPa for a 20 cm clast; Eppes et al., 2016), well below commonly reported ranges for the tensile strength of limestones (e.g., $\sim$2–15 MPa; Arjmandpour and Hosseinitoudeshki, 2013; Nazir et al., 2013).

The Role of Water in Progressive Fracturing

Previous studies demonstrated that the time-progressive subaerial diminution of clast sizes on the late Quaternary terrace surfaces of Shehoret was governed by a rock fragmentation process (Mushkin et al., 2014). Herein we suggest that this fragmentation was driven by progressive fracturing over geologic time and that water may have been involved in setting the rate of this fracturing. Petrographic observations (Fig. 7D) indicate that the characteristic "sugary" texture of the fracture Outer Zone and the clast exterior is associated with selective dissolution of the micritic limestone matrix, which surrounds the larger, more resistant, sand-size dolomite rhomb crystals. We propose that this selective dissolution may also occur along the fracture surface resulting in the release of dolomite rhombs into the loose material of the fracture Accumulation Zone (Fig. 5C). In addition, the SEM images consistently reveal dissolution morphologies along all three natural fracture zones (Figs. 8D–8F) and up to the crack-tip (Fig. 9B), indicating the presence of water and suggesting hydraulic connectivity between the inner fracture segments and the external environment (Fig. 4).

Further support for the presence of water in the fractures of the Shehoret clasts is found in the presence of allochthonous (foreign) elements such as aluminum, silicon, and iron at the crack-tip process zone (Figs. 5F–5H and 6D). Specifically, the occurrence of allochthonous elements in the process zone (beyond the reach of aeolian dust into the fracture filling) suggests that microfracturing there may allow water access to rock ahead of the tip before it is a fully developed fracture segment, transporting with it foreign elements sourced from the dust of the Accumulation Zone. Thus, mobility of foreign elements into the rock along all the fracture zones indicates a hydraulically connected system along the fracture that not only reaches the crack-tip but also extends beyond into the process zone. Once water enters the fracture, conditions within the fracture including dust of the Accumulation Zone may facilitate the extended persistence of liquid water or water vapor at the crack-tip. Once such water is locked into the fracture process zone, fracturing processes related to thermal stresses can still occur. Subcritical cracking is significantly accelerated when humidity is higher due to the chemo-physical nature of bond breakage (e.g., Dove, 1995). Physical modeling of the impact of moisture on the rates of long-term rock fracturing that occurs due to thermal stresses suggests orders of magnitude faster fracturing in more humid environments under identical driving stresses (Eppes and Keanini, 2017). Accordingly, our findings provide unique field-based indications for the intimate role of water in subcritical cracking, which has been previously well documented in the laboratory both generally (Brantut et al., 2012) and specifically for carbonate rocks (e.g., Nara et al., 2017), as well as in "real time" measurements in a field-based experiment (Eppes et al., 2020).

We suggest that this linkage between moisture availability and the rates of mechanical rock weathering occurring through progressive, subcritical cracking can be key in the understanding of hyper-arid landscapes where mechanical weathering is dominant and moisture availability is overall extremely limited, but still present. Relatively small changes in moisture conditions, such as those possibly imposed due to ongoing climate changes, could result in disproportionate changes in fracturing rates and surface weathering. If fracturing is occurring subcritically, then changes in externally applied stresses may not be necessary to change natural fracturing rates, as changes in environmental conditions (e.g., moisture) at the crack-tip could be sufficient.

CONCLUSIONS

In this work, we describe field-based observations that consistently suggest that fractures found in dolomitized micritic limestone clasts in the hyper-arid environment of the Dead Sea Rift Valley opened progressively over geologic time scales, rather than as a single dynamic fracture event. The field measurements revealed a monotonic increase in fracture number density with increasing surface age, and thus inferred continuous growth of the fracture network through geologic time. Additional field observations, petrographic, SEM, and micron-scale roughness analyses of individual fracture surfaces, show that surfaces of the fractures in the examined clasts were marked by a characteristic weathering zonation that reflects geologic time differences between the most weathered fracture surfaces found near the clast exterior and the most pristine fracture surfaces found in the clast interior. In addition, we propose that the dominantly intergranular nature of the natural fracture pathways is suggestive of subcritical propagation of the fractures in the clasts examined but acknowledge that fractures could have also formed step-wise in small increments. The surfaces of fractures that propagated dynamically in the same samples (induced by hammer and chisel) were smoother than natural fracture surfaces, and dominantly crosscut through crystals. SEM analyses revealed evidence for both dissolution textures and water-mediated penetration of allochthonous elements such as aluminum, silicon, and iron along the fracture surfaces and beyond into the crack-tip process zone. These indications for hydraulic connectivity along fracture surfaces and beyond the crack-tip provide field-based support for the previously proposed role of moisture as a rate-setting factor for mechanical weathering driven by subcritical cracking over geologic time scales. That natural rock fracturing can be a progressive process has implications across other earth science disciplines. If the rates of progressive fracturing

change over time, then so could rates of any subsequent or dependent process predicated on rock fracture.

ACKNOWLEDGMENTS

Danny Shaanan is acknowledged for providing computing data solutions. Fieldwork was assisted by Naama Gros, Annya Zafrunski, Noa Jeselsohn, Nimrod Wieler, and Danny Shaanan. Insightful reviews by Peter Eichhubl (associate editor) and two anonymous reviewers significantly improved the manuscript. The work was funded by U.S.-Israel Binational Science Foundation Award #2018610 and National Science Foundation (NSF) Division of Earth Sciences (EAR) award #1839148 to A. Mushkin, M.-C. Eppes, and R. Keanini.

REFERENCES CITED

Adelsberger, K.A., and Smith, J.R., 2009, Desert pavement development and landscape stability on the Eastern Libyan Plateau, Egypt: Geomorphology, v. 107, no. 3-4, p. 178–194, https://doi.org/10.1016/j.geomorph.2008.12.005.

Aldred, J., Eppes, M.C., Aquino, K., Deal, R., Garbini, J., Swami, S., Tuttle, A., and Xanthos, G., 2016, The influence of solar-induced thermal stresses on the mechanical weathering of rocks in humid mid-latitudes: Earth Surface Processes and Landforms, v. 41, no. 5, p. 603–614, https://doi.org/10.1002/esp.3849.

Amit, R., and Gerson, R., 1986, The evolution of Holocene reg (gravelly) soils in deserts: An example from the dead sea region: Catena, v. 13, no. 1–2, p. 59–79, https://doi.org/10.1016/S0341-8162(86)80005-4.

Amit, R., Gerson, R., and Yaalon, D., 1993, Stages and rate of the gravel shattering process by salts in desert Reg soils: Geoderma, v. 57, p. 295–324, https://doi.org/10.1016/0016-7061(93)90011-9.

Amit, R., Harrison, J.B.J., Enzel, Y., and Porat, N., 1996, Soils as a tool for estimating ages of Quaternary fault scarps in a hyperarid environment: The southern Arava valley, the Dead Sea Rift, Israel: Catena, v. 28, no. 1–2, p. 21–45, https://doi.org/10.1016/S0341-8162(96)00028-8.

Amit, R., Enzel, Y., and Sharon, D., 2006, Permanent Quaternary hyperaridity in the Negev, Israel, resulting from regional tectonics blocking Mediterranean frontal systems: Geology, v. 34, p. 509–512, https://doi.org/10.1130/G22354.1.

Arjmandpour, J., and Hosseinitoudeshki, V., 2013, Estimation of tensile strength of limestone from some of its physical properties via simple regression: Journal of Novel Applied Sciences, v. 2, no. S3, p. 1041–1044.

Atkinson, B.K., 1982, Subcritical crack propagation in rocks: Theory, experimental results and applications: Journal of Structural Geology, v. 4, no. 1, p. 41–56, https://doi.org/10.1016/0191-8141(82)90005-0.

Atkinson, B.K., 1984, Subcritical crack growth in geological materials: Journal of Geophysical Research: Solid Earth, v. 89, no. B6, p. 4077–4114, https://doi.org/10.1029/JB089iB06p04077.

Atkinson, B.K., ed., 1987, Fracture Mechanics of Rock: London, UK, Academic Press, 534 p., https://doi.org/10.1016/C2009-0-21691-6.

Barnett, R., and Kerrich, R., 1980, Stress corrosion cracking of biotite and feldspar: Nature, v. 283, p. 185–187, https://doi.org/10.1038/283185a0.

Barzilai, E., Enzel, Y., and Amit, R., 2000, Constructing synthetic time-series of rainfall events for environmental modeling in a hyperarid environment, Southern Arava, Israel: International Association of Hydrological Sciences (IAHS), v. 261, p. 29–42.

Ben-Israel, M., Enzel, Y., Amit, R., and Erel, Y., 2015, Provenance of the various grain-size fractions in the Negev loess and potential changes in major dust sources to the Eastern Mediterranean: Quaternary Research, v. 83, no. 1, p. 105–115, https://doi.org/10.1016/j.yqres.2014.08.001.

Beyth, M., Eyal, Y., and Garfunkel, Z., 2012, Geological map of Israel: Jerusalem, Elat. Israel Geological Survey, scale 1:50,000, sheet 26 (partly revised, 2018).

Bost, M., and Pouya, A., 2017, Stress generated by the freeze–thaw process in open cracks of rock walls: Empirical model for tight limestone: Bulletin of Engineering Geology and the Environment, v. 76, p. 1491–1505, https://doi.org/10.1007/s10064-016-0955-6.

Brantut, N., Baud, P., Heap, M., and Meredith, P., 2012, Micromechanics of brittle creep in rocks: Journal of Geophysical Research: Solid Earth, v. 117, no. B8, p. 1978–2012.

Bull, W.B., 1977, The alluvial-fan environment: Progress in Physical Geography, v. 1, no. 2, p. 222–270, https://doi.org/10.1177/030913337700100202.

Chen, X., Eichhubl, P., Olson, J.E., and Dewers, T., 2019, Effect of water on fracture mechanical properties of shales: Journal of Geophysical Research: Solid Earth, v. 124, p. 2428–2444, https://doi.org/10.1029/2018JB016479.

Chen, X., Eichhubl, P., Olson, J.E., and Dewers, T.A., 2020, Salinity, pH, and temperature controls on fracture mechanical properties of three shales and their implications for fracture growth in chemically reactive fluid environments: Geomechanics for Energy and the Environment, v. 21, https://doi.org/10.1016/j.gete.2019.100140.

Collins, B.D., and Stock, G.M., 2016, Rockfall triggering by cyclic thermal stressing of exfoliation fractures: Nature Geoscience, v. 9, no. 5, p. 395–400, https://doi.org/10.1038/ngeo2686.

Cooke, R.U., 1970, Stone pavements in deserts: Annals of the Association of American Geographers, v. 60, no. 3, p. 560–577, https://doi.org/10.1111/j.1467-8306.1970.tb00741.x.

Crouvi, O., Barzilai, O., Goldsmith, Y., Amit, R., Matskevich, Z., Porat, N., and Enzel, Y., 2018, Middle to late Pleistocene shift in eolian silts contribution into Mediterranean soils at the fringe of the Negev loess, Israel: Quaternary Science Reviews, v. 191, p. 101–117, https://doi.org/10.1016/j.quascirev.2018.04.030.

Dan, J., Yaalon, D.H., Moshe, R., and Nissim, S., 1982, Evolution of reg soils in southern Israel and Sinai: Geoderma, v. 28, no. 3–4, p. 173–202, https://doi.org/10.1016/0016-7061(82)90002-7.

D'Arcy, M., Roda Boluda, D.C., Whittaker, A.C., and Carpineti, A., 2015, Dating alluvial fan surfaces in Owens Valley, California, using weathering fractures in boulders: Earth Surface Processes and Landforms, v. 40, p. 487–501, https://doi.org/10.1002/esp.3649.

Doehne, E., 2002, Salt weathering: A selective review: Geological Society, London, Special Publication 205, p. 51–64, https://doi.org/10.1144/GSL.SP.2002.205.01.05.

Dove, P.M., 1995, Geochemical controls on the kinetics of quartz fracture at subcritical tensile stresses: Journal of Geophysical Research: Solid Earth, v. 100, no. B11, p. 22,349–22,359, https://doi.org/10.1029/95JB02155.

Eppes, M.C., and Keanini, R., 2017, Mechanical weathering and rock erosion by climate-dependent subcritical cracking: Reviews of Geophysics, v. 55, p. 470–508, https://doi.org/10.1002/2017RG000557.

Eppes, M.C., McFadden, L.D., Wegmann, K.W., and Scuderi, L.A., 2010, Cracks in desert pavement rocks: Further insights into mechanical weathering by directional insolation: Geomorphology, v. 123, no. 1–2, p. 97–108, https://doi.org/10.1016/j.geomorph.2010.07.003.

Eppes, M.C., Willis, A., Molaro, J., Abernathy, S., and Zhou, B., 2015, Cracks in Martian boulders exhibit preferred orientations that point to solar-induced thermal stress: Nature Communications, v. 6, 6712, https://doi.org/10.1038/ncomms7712.

Eppes, M.C., Magi, B., Hallet, B., Delmelle, E., Mackenzie-Helnwein, P., Warren, K., and Swami, S., 2016, Deciphering the role of solar-induced thermal stresses in rock weathering: Geological Society of America Bulletin, v. 128, p. 1315–1338, https://doi.org/10.1130/B31422.1.

Eppes, M.C., Hancock, G.S., Chen, X., Arez, J., Dewers, T., Huettenmoser, J., Kiessling, S., Moser, F., Tannu, N., Weiserbs, B., and Whitten, J., 2018, Rates of subcritical cracking and long-term rock erosion: Geology, v. 46, p. 951–954, https://doi.org/10.1130/G45256.1.

Eppes, M.C., Magi, B., Scheff, J., Warren, K., Ching, S., and Feng, T., 2020, Warmer, wetter climates accelerate mechanical weathering in field data, independent of stress-loading: Geophysical Research Letters, v. 47, no. 24, https://doi.org/10.1029/2020GL089062.

Greenbaum, N., Schwartz, U., Carling, P., Bergman, N., Mushkin, A., Zituni, R., Halevi, R., Benito, G., and Porat, N., 2020, Frequency of boulders transport during large floods in hyperarid areas using paleoflood analysis: An example from the Negev Desert, Israel: Earth-Science Reviews, v. 202, https://doi.org/10.1016/j.earscirev.2020.103086.

Gregg, J.M., and Sibley, D.F., 1984, Epigenetic dolomitization and the origin of xenotopic dolomite texture: Journal of Sedimentary Research, v. 54, no. 3, p. 908–931.

Griffith, A.A., 1921, The phenomena of rupture and flow in solids: Philosophical Transactions of the Royal Society of London, v. 221, p. 163–198, https://doi.org/10.1098/rsta.1921.0006.

Hetz, G., Mushkin, A., Blumberg, D.G., Baer, G., and Ginat, H., 2016, Estimating the age of desert alluvial surfaces with spaceborne radar data: Remote Sensing of Environment, v. 184, p. 288–301, https://doi.org/10.1016/j.rse.2016.07.006.

Huggett, R.J., 1998, Soil chronosequences, soil development, and soil evolution: A critical review: Catena, v. 32, p. 155–172.

Jaeger, J.C., Cook, N.G., and Zimmerman, R., 2009, Fundamentals of rock mechanics: Hoboken, New Jersey, USA, John Wiley & Sons, 488 p.

Jiménez-González, I., Rodríguez-Navarro, C., and Scherer, G.W., 2008, Role of clay minerals in the physicomechanical deterioration of sandstone: Journal of Geophysical Research: Earth Surface, v. 113, no. F2, https://doi.org/10.1029/2007JF000845.

Kerrich, R., La Tour, T.E., and Barnett, R.L., 1981, Mineral reactions participating in intragranular fracture propagation: Implications for stress corrosion cracking: Journal of Structural Geology, v. 3, no. 1, p. 77–87, https://doi.org/10.1016/0191-8141(81)90058-4.

Kudo, Y., Sano, O., Murashige, N., Mizuta, Y., and Nakagawa, K., 1992, Stress-induced crack path in Aji granite under tensile stress: Pure and Applied Geophysics, v. 138, no. 4, p. 641–656, https://doi.org/10.1007/BF00876342.

Laubach, S.E., Eichhubl, P., Hilgers, C., and Lander, R.H., 2010, Structural diagenesis: Journal of Structural Geology, v. 32, no. 12, p. 1866–1872, https://doi.org/10.1016/j.jsg.2010.10.001.

Laubach, S.E., et al., 2019, The role of chemistry in fracture pattern development and opportunities to advance interpretations of geological materials: Reviews of Geophysics, v. 57, no. 3, p. 1065–1111, https://doi.org/10.1029/2019RG000671.

Lawn, B., and Wilshaw, R., 1975, Indentation fracture: Principles and applications: Journal of Materials Science, v. 10, p. 1049–1081, https://doi.org/10.1007/BF00823224.

Marder, M., and Fineberg, J., 1996, How things break: Physics Today, v. 49, no. 9, p. 24–29, https://doi.org/10.1063/1.881515.

Martel, S.J., 2017, Progress in understanding sheeting joints over the past two centuries: Journal of Structural Geology, v. 94, p. 68–86, https://doi.org/10.1016/j.jsg.2016.11.003.

McFadden, L.D., Ritter, J.B., and Stephen, G.W., 1989, Use of multiparameter relative-age methods for age estimation and correlation of alluvial fan surfaces on a desert piedmont, eastern Mojave Desert, California: Quaternary Research, v. 32, no. 3, p. 276–290, https://doi.org/10.1016/0033-5894(89)90094-X.

McFadden, L.D., McDonald, E.V., Wells, S.G., Anderson, K., Quade, J., and Forman, S.L., 1998, The vesicular layer and carbonate collars of desert soils and pavements: Formation, age and relation to climate change: Geomorphology, v. 24, no. 2–3, p. 101–145, https://doi.org/10.1016/S0169-555X(97)00095-0.

McFadden, L.D., Eppes, M., Gillespie, A., and Hallet, B., 2005, Physical weathering in arid landscapes due to diurnal variation in the direction of solar heating: Geological Society of America Bulletin, v. 117, p. 161–173, https://doi.org/10.1130/B25508.1.

Meredith, P.G., and Atkinson, B.K., 1981, Acoustic emission and stress corrosion of Whin Sill dolerite: Progress in Experimental Petrology, v. 5, p. 293–295.

Meredith, P.G., and Atkinson, B.K., 1983, Stress corrosion and acoustic emission during tensile crack propagation in Whin Sill dolerite and other basic rocks: Geophysical Journal International, v. 75, no. 1, p. 1–21, https://doi.org/10.1111/j.1365-246X.1983.tb01911.x.

Molnar, P., 2004, Interactions among topographically induced elastic stress, static fatigue, and valley incision: Journal of Geophysical Research: Earth Surface, v. 109, no. F2, https://doi.org/10.1029/2003JF000097.

Morad, D., Sagy, A., Tal, Y., and Hatzor, Y.H., 2022, Fault roughness controls sliding instability: Earth and Planetary Science Letters, v. 579, https://doi.org/10.1016/j.epsl.2022.117365.

Murton, J.B., Peterson, R., and Ozouf, J.C., 2006, Bedrock fracture by ice segregation in cold regions: Science, v. 314, no. 5802, p. 1127–1129, https://doi.org/10.1126/science.1132127.

Mushkin, A., Sagy, A., Trabelci, E., Amit, R., and Porat, N., 2014, Measuring the time and scale-dependency of subaerial rock weathering rates over geologic time scales with ground-based lidar: Geology, v. 42, p. 1063–1066, https://doi.org/10.1130/G35866.1.

Nara, Y., and Kaneko, K., 2005, Study of subcritical crack growth in andesite using Double Torsion test: International Journal of Rock Mechanics and Mining Sciences, v. 42, no. 4, p. 521–530, https://doi.org/10.1016/j.ijrmms.2005.02.001.

Nara, Y., Koike, K., Yoneda, T., and Kaneko, K., 2006, Relation between subcritical crack growth behavior and crack paths in granite: International Journal of Rock Mechanics and Mining Sciences, v. 43, no. 8, p. 1256–1261, https://doi.org/10.1016/j.ijrmms.2006.03.016.

Nara, Y., Morimoto, K., Hiroyoshi, N., Yoneda, T., Kaneko, K., and Benson, P.M., 2012, Influence of relative humidity on fracture toughness of rock: Implications for subcritical crack growth: International Journal of Solids and Structures, v. 49, p. 2471–2481, https://doi.org/10.1016/j.ijsolstr.2012.05.009.

Nara, Y., Kashiwaya, K., Nishida, Y., and Ii, T., 2017, Influence of surrounding environment on subcritical crack growth in marble: Tectonophysics, v. 706–707, p. 116–128, https://doi.org/10.1016/j.tecto.2017.04.008.

Nazir, R., Momeni, E., Armaghani, D.J., and Amin, M.M., 2013, Correlation between unconfined compressive strength and indirect tensile strength of limestone rock samples: The Electronic Journal of Geotechnical Engineering, v. 18, no. 1, p. 1737–1746.

Olsen, T., Borella, J., and Stahl, T., 2020, Clast transport history influences Schmidt hammer rebound values: Earth Surface Processes and Landforms, v. 45, no. 6, p. 1392–1400, https://doi.org/10.1002/esp.4809.

Olson, J.E., Laubach, E.S., and Lander, R.H., 2009, Natural fracture characterization in tight gas sandstones: Integrating mechanics and diagenesis: AAPG Bulletin, v. 93, no. 11, p. 1535–1549, https://doi.org/10.1306/08110909100.

Porat, N., Amit, R., Enzel, Y., Zilberman, E., Avni, Y., Ginat, H., and Gluck, D., 2010, Abandonment ages of alluvial landforms in the hyperarid Negev determined by luminescence dating: Journal of Arid Environments, v. 74, no. 7, p. 861–869, https://doi.org/10.1016/j.jaridenv.2009.10.018.

Ravaji, B., Lagoa, V.A., Delbo, M., and Wilkerson, J., 2019, Unraveling the mechanics of thermal stress weathering: Rate-effects, size-effects, and scaling laws: Journal of Geophysical Research: Planets, v. 124, no. 12, p. 3304–3328, https://doi.org/10.1029/2019JE006019.

Rimsza, J.M., Jones, R.E., and Criscenti, L.J., 2018, Chemical effects on subcritical fracture in silica from molecular dynamics simulations: Journal of Geophysical Research: Solid Earth, v. 123, p. 9341–9354, https://doi.org/10.1029/2018JB016120.

Stevens, P.R., and Walker, T.W., 1970, The chronosequence concept and soil formation: The Quarterly Review of Biology, v. 45, no. 4, p. 333–350, https://doi.org/10.1086/406646.

Stock, G.M., Martel, S.J., Collins, B.D., and Harp, E.L., 2012, Progressive failure of sheeted rock slopes: The 2009–2010 Rhombus Wall rock falls in Yosemite Valley, California, USA: Earth Surface Processes and Landforms, v. 37, no. 5, p. 546–561, https://doi.org/10.1002/esp.3192.

Swanson, P.L., 1984, Subcritical crack growth and other time-and environment-dependent behaviour in crustal rocks: Journal of Geophysical Research: Solid Earth, v. 89, no. B6, p. 4137–4152, https://doi.org/10.1029/JB089iB06p04137.

Voigtländer, A., Leith, K., and Krautblatter, M., 2018, Subcritical crack growth and progressive failure in Carrara marble under wet and dry conditions: Journal of Geophysical Research: Solid Earth, v. 123, p. 3780–3798, https://doi.org/10.1029/2017JB014956.

Walder, J., and Hallet, B., 1985, A theoretical model of the fracture of rock during freezing: Geological Society of America Bulletin, v. 96, p. 336–346, https://doi.org/10.1130/0016-7606(1985)96<336:ATMOTF>2.0.CO;2.

Wells, S.G., McFadden, L.D., Poths, J., and Olinger, C.T., 1995, Cosmogenic 3He surface-exposure dating of stone pavements: Implications for landscape evolution in deserts: Geology, v. 23, p. 613–616, https://doi.org/10.1130/0091-7613(1995)023<0613:CHSEDO>2.3.CO;2.

Science Editor: Brad Singer
Associate Editor: Peter Eichhubl

Manuscript Received 9 July 2022
Revised Manuscript Received 29 March 2023
Manuscript Accepted 17 April 2023

Printed in the USA